ChemistryOPEN

Supporting Information

Insights into the Binding of Cyclic RGD Peptidomimetics to $\alpha_5\beta_1$ Integrin by using Live-Cell NMR And Computational Studies

Ileana Guzzetti,[a] Monica Civera,[a] Francesca Vasile,[a] Daniela Arosio,[b] Cristina Tringali,[c] Umberto Piarulli,[d] Cesare Gennari,[a] Luca Pignataro,[a] Laura Belvisi,*[a] and Donatella Potenza*[a]

open_201600112_sm_miscellaneous_information.pdf

Table of Contents

Docking model of α5β1 integrin

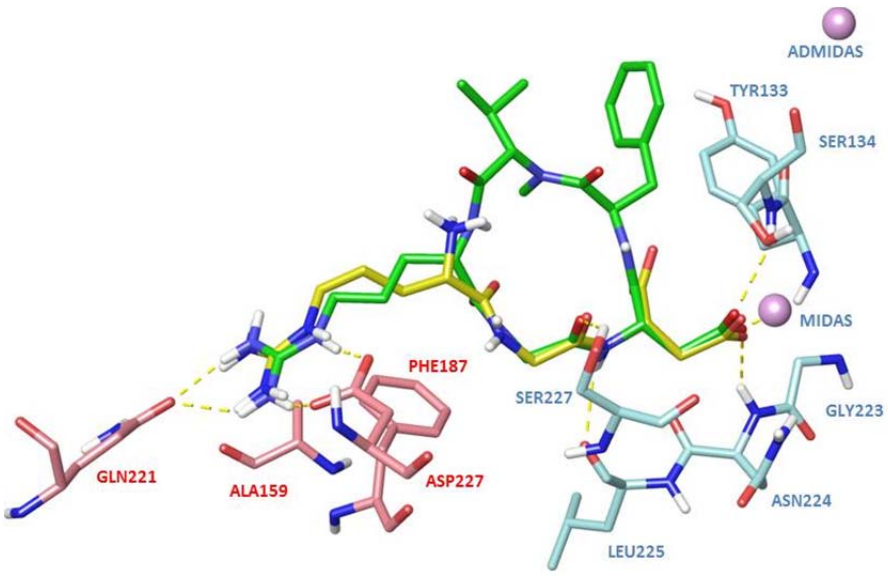

Figure S1. Docking best pose of Cilengitide (green) in the crystal structure of the extracellular domain of α5β1 integrin (α5 subunit pink, β1 subunit cyan, model from 3VI4.pdb) overlaid on the X-ray structure of the linear RGD peptide (yellow). Only selected integrin residues involved in interactions with the ligand are shown. Non polar hydrogens are hidden for clarity, while intermolecular hydrogen bonds are shown as dashed lines.

Free state conformational analysis

The conformational studies of the cyclic RGD peptidomimetics containing the DKP scaffolds have been previously performed by means of ^{1}H NMR spectroscopy experiments in phosphate buffer solution and Monte Carlo/Stochastic Dynamics (MC/SD) simulations restrained by long-range NOE contacts (OPLS_2001 force field, implicit water GB/SA solvation model).[1] On the basis of these studies, four preferred intramolecular H-bonding patterns have been identified and denoted as type I – IV (Figure S2). Each H-bonding pattern is characterized by a β-turn (vide infra), but in addition the formation of specific γ-turns is observed during the simulations.

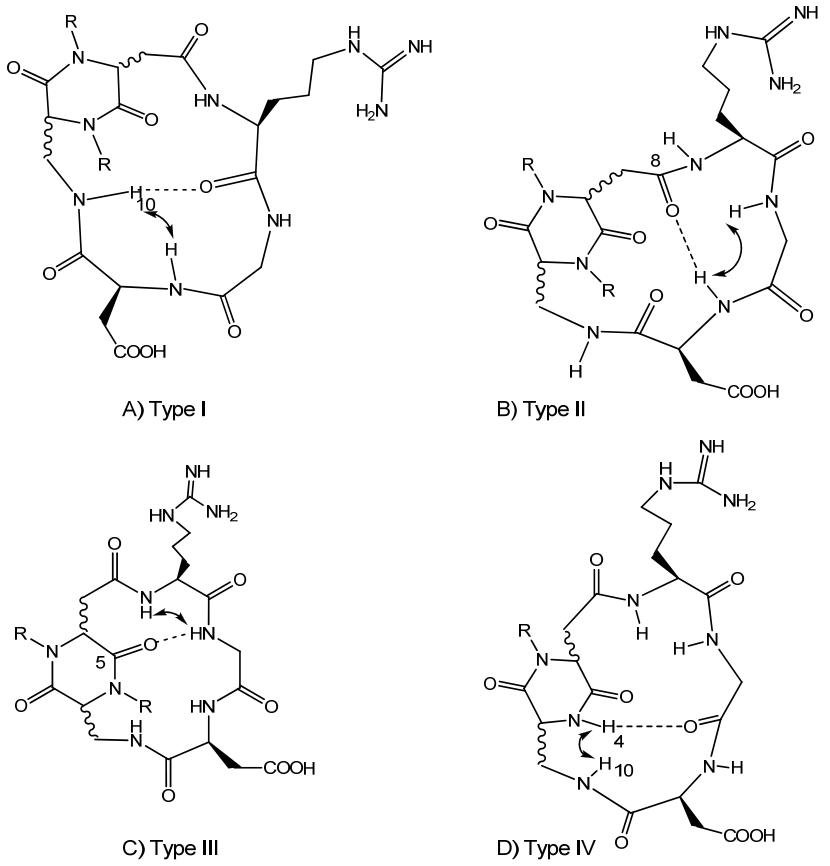

Figure S2. Preferred intramolecular hydrogen-bonded patterns identified for the cyclic [DKP-RGD] peptidomimetics on the basis of NMR and computational studies. The arrows indicate significant NOE contacts and the dotted lines the intramolecular hydrogen bonds. A) Type I H-bonding pattern, β-turn at Gly-Asp. B) Type II H-bonding pattern, β-turn at Arg-Gly. C) Type III H-bonding pattern, pseudo-β-turn at DKP-Arg. D) Type IV H-bonding pattern, pseudo-β-turn at Asp-DKP.

[1] M. Marchini, M. Mingozzi, R. Colombo, I. Guzzetti, L. Belvisi, F. Vasile, D. Potenza, U. Piarulli, D. Arosio, C. Gennari, Chem. Eur. J. 2012, 18, 6195 – 6207.

The type I H-bonding pattern is characterized by a β-turn motif at Gly-Asp stabilized by a hydrogen bond between DKP-NH10 and Arg-C=O and, generally, the NH10-NHAsp NOE contact is observed. The type II H-bonding pattern is described by a β-turn motif at Arg-Gly stabilized by a hydrogen bond between Asp-NH and C(8)=O and, typically, characterized by the NHAsp-NHGly NOE contact. The type III H-bonding pattern is defined by a pseudo-β-turn motif at DKP-Arg, stabilized by a hydrogen bond between NHGly and C(5)=O and the NHGly-NHArg NOE contact is detectable. Finally, the type IV H-bonding pattern is characterized by a pseudo β-turn motif at Asp-DKP, stabilized by a hydrogen bond between NH4 and Gly-C=O (NOE contact between NH4 and NH10).

Conformational studies of compounds **2-7** revealed that the ligands display well-defined preferred conformations characterized by intramolecular hydrogen-bonded turn motifs and an extended arrangement of the RGD sequence [Cβ(Arg)-Cβ(Asp) average distances of about 9 Å]. In particular, compounds **2**, **3** and **5** preferentially adopted the type III conformation characterized by the pseudo-β-turn at DKP-Arg and the formation of the corresponding hydrogen bond between the NHGly and C(5)=O. In fact, the NOESY spectra of these ligands showed only one relevant long-range contact between NHGly and NHArg. The distance restraint corresponding to this NOE contact was applied in the MC/SD simulations and most of the conformations sampled during these simulations adopted an extended arrangement of the RGD sequence characterized by the pseudo-β-turn at DKP-Arg and the formation of the corresponding hydrogen bond between the NHGly and C(5)=O. In addition, the formation of a γ-turn at Asp stabilized by the hydrogen bond between NH10 and Gly-C=O is observed during the simulations. A representative energy minimized conformation selected by cluster analysis and featuring the type III H-bonding pattern is shown in Figure S3 for the RGD peptidomimetic **3**.

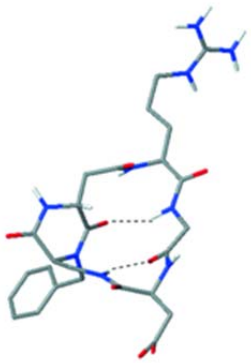

Figure S3. Type III conformation of compound **3** as obtained by restrained MC/SD simulations based on experimental distance information, after energy minimization (inverse γ-turn at Asp and pseudo-β-turn at DKP-Arg, Cβ(Arg)-Cβ(Asp) = 8.8 Å).

Conversely, compounds **4, 6** and **7** preferentially adopted the type I conformation characterized by the β-turn at Gly-Asp and the formation of the corresponding hydrogen bond between DKP-NH10 and Arg-C=O (and, generally, by the NH10-NHAsp NOE contact). The contribution of a second conformation (the type IV characterized by the pseudo-β-turn at Asp-DKP and the hydrogen bond between DKP-NH_4 and Gly-C=O, see Figure S2) to the free state conformational equilibrium of ligand **6** was suggested by NMR spectroscopy data (moderate NOE contact involving NH4 and NH10 observed in the NOESY spectrum). Accordingly, three-dimensional structures satisfying long-range NOE contacts were generated for ligand **6** by performing two restrained MC/SD simulations and applying the DKP-NH10/NHAsp or the NH4/NH10 distance restraint derived from NOESY spectra. Most of the conformations sampled during the first simulation adopted an extended arrangement of the RGD sequence and are characterized by the β-turn at Gly-Asp and the corresponding hydrogen bond between DKP-NH10 and Arg-C=O. In addition, the formation of a γ-turn at Asp stabilized by the hydrogen bond between NH10 and Gly-C=O is observed during the simulation. A representative energy minimized conformation selected by cluster analysis and featuring these H bond is shown in Figure S4-A (type I H bonding pattern). Most of the conformations sampled during the simulation of **6** applying the NH4/NH10 distance restraint adopted an extended arrangement of the RGD sequence and are characterized by the pseudo-β-turn at Asp-DKP and the corresponding hydrogen bond between NH4 and Gly-C=O. In addition, the formation of a γ-turn at Asp stabilized by the hydrogen bond between NH10 and Gly-C=O is observed during the simulation. A representative energy minimized conformation selected by cluster analysis and featuring these H bonds is shown in Figure S4-B (type IV H-bonding pattern).

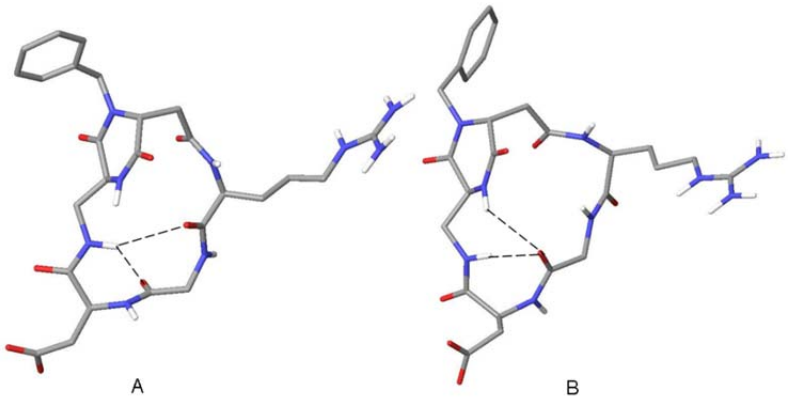

Figure S4. Structures of **6** as obtained by restrained MC/SD simulations based on experimental distance information, after energy minimization. A) Type I conformation (inverse γ-turn at Asp and distorted βII'-turn at Gly-Asp, Cβ(Arg)-Cβ(Asp) = 9.0 Å). B) Type IV conformation (inverse γ-turn at Asp and pseudo-β-turn at Asp-DKP, Cβ(Arg)-Cβ(Asp) = 8.8 Å).

Docking poses of compound 4

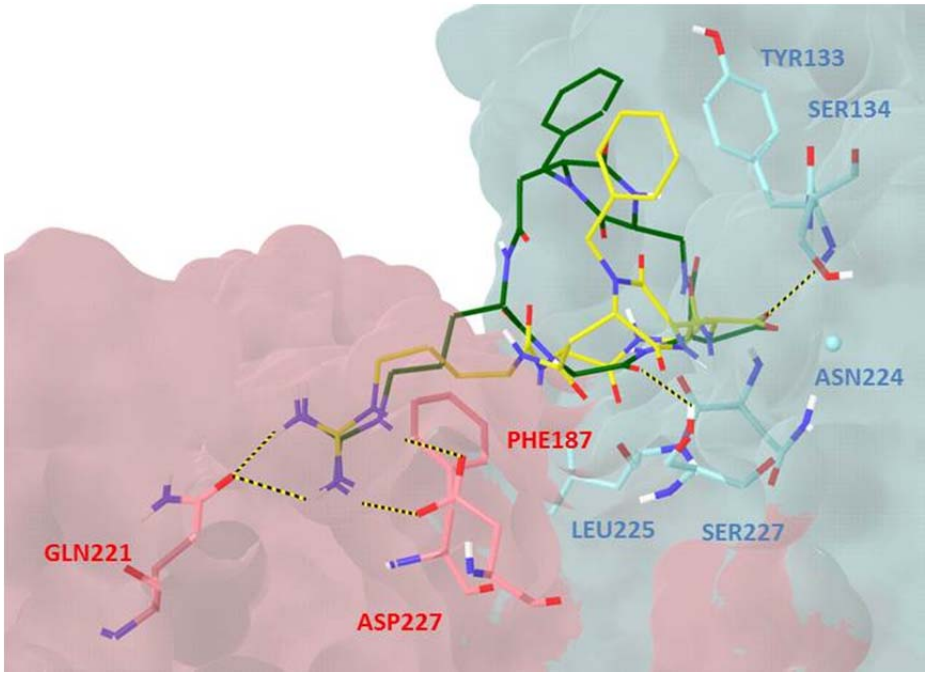

Figure S5. Docking best pose (green) and second pose (yellow) of compound **4** in the crystal structure of the extracellular domain of α5β1 integrin (α5 subunit pink, β1 subunit cyan, model from 3VI4.pdb). Only selected integrin residues involved in interactions with the ligand are shown. Non polar hydrogens are hidden for clarity, while intermolecular hydrogen bonds are shown as dashed lines.

Tables of ^{1}H chemical shifts of compounds 2-7

Tables S1-S6. ^{1}H chemical shifts δ (ppm), signal multiplicity and coupling constant (Hz) of compounds **2-7** in phosphate buffer solution (pH 7.2) in the presence of MDA-MB-231 cell suspension at T= 283 K.

Compound **2** / Protons	δ (multiplicity, J)
NH_Arg	8.68 (d, 6.6Hz)
αH-Arg	4.18 (m)
βH-Arg	1.76 (m) ; 1.67 (m)
γH-Arg	1.60 (m)
δH-Arg	3.13 (t, 5.23 Hz)
NH_guan	7.16 (bs)
NH_Gly	8.22 (d, 9.67 Hz)
αH-Gly	4.12 (m) ; 3.45 (d, 15.6 Hz)
NH_Asp	8.36 (d, 8.14 Hz)
αH-Asp	4.60 (m)
βH-Asp	2.57 (dd, 16.5-8 Hz) ; 2.47 (dd, 16.5-7.4 Hz)
DKP_NH1	8.45 (s)
DKP_NH10	8.75 (dd, 9.7-4.1 Hz)
DKP_H9	4.26 (m) ; 3.29 (d, 16.8 Hz)
DKP_H3	4.15 (m)
DKP_H7	2.84 (dd, 14.2 – 9.7 Hz) ; 2.35 (d, 14.2 Hz)
DKP_H6	4.63 (m)
CH_2-Bn	5.05 (bs) ; 4.14 (m)
H-Ar	7.40-7.25

Compound **3** / Protons	δ (multiplicity, J)
NH_Arg	8.79 (d, 8.44 Hz)
αH-Arg	4.26 (m)
βH-Arg	1.87 (m) ; 1.69 (m)
γH-Arg	1.57 (m)
δH-Arg	3.13 (m)
NH_guan	7.16 (t, 5.50 Hz)
NH_Gly	8.12 (m)
αH-Gly	4.19 (dd, 17.80-8.15 Hz) ; 3.60 (dd, 17.80- 4.34 Hz)
NH_Asp	8.05 (d, 8.61 Hz)
αH-Asp	4.66 (m)
βH-Asp	2.54 (m)
DKP_NH1	8.15 (s)
DKP_NH10	8.28 (t, 6.36 Hz)
DKP_H9	3.93 (dd, 15.48-7.23Hz) ; 3.53 (dt, 15.48-6.42 Hz)
DKP_H3	4.03 (m)
DKP_H7	2.76 (dd, 14.29-8.80 Hz) ; 2.63 (dd, 14.29-5.28 Hz)
DKP_H6	4.67 (m)
CH_2-Bn	5.05 (m) ; 4.05 (m)
H-Ar	7.40-7.20

Compound **4** / Protons	δ (multiplicity, J)
NH_Arg	8.42 (d, 5.92 Hz)
αH-Arg	4.23 (m)
βH-Arg	1.78 (m) ; 1.68 (m)
γH-Arg	1.58 (m)
δH-Arg	3.11 (t, 5.96 Hz)
NH_guan	7.16 (bs)
NH_Gly	8.35 (t, 5.92 Hz)
αH-Gly	3.96 (m) ; 3.59 (m)
NH_Asp	8.84 (bs)
αH-Asp	4.21 (m)
βH-Asp	2.60 (dd, 16.71-4.05 Hz) ; 2.51(dd, 16.71-10.38 Hz)
DKP_NH4	8.29 (s)
DKP_NH10	7.49 (d, 9.86 Hz)
DKP_H9	3.67 (m) ; 3.23 (m)
DKP_H3	3.81 (m)
DKP_H7	2.99 (d, 17.04 Hz) ; 2.74 (d, 17.04 Hz)
DKP_H6	4.16 (bs)
CH_2-Bn	5.16 (d, 16.7 Hz) ; 4.10 (d, 16.7 Hz)
H-Ar (2)	7.35 - 7.20

Compound **5** / Protons	δ (multiplicity, J)
NH_Arg	8.38 (d, 6.91 Hz)
αH-Arg	3.90 (m)
βH-Arg	1.54 (m) ; 1.42 (m)
γH-Arg	1.36 (m)
δH-Arg	2.92 (m)
NH_guan	6.93 (m)
NH_Gly	8.06 (d, 10.18 Hz)
αH-Gly	4.04 (dd, 16.00-10.18 Hz) ; 3.20 (d, 16.00 Hz)
NH_Asp	8.23 (d, 8.42 Hz)
αH-Asp	4.48 (m)
βH-Asp	2.39 (dd, 15.93-7.54 Hz) ; 2.25 (dd, 15.93-7.75 Hz)
DKP_NH10	8.44 (dd, 9.32- 4.51 Hz)
DKP_H9	4.14 (m) ; 3.14 (dd, 14.54-4.51 Hz)
DKP_H3	4.42 (m)
DKP_H7	2.30 (m)
DKP_H6	4.18 (m)
CH_2-Bn	4.96 (d, 17.45 Hz) ; 4.16 (m)
CH_2-Bn	4.83 (m) ; 3.99 (d, 15.27 Hz)
H-Ar (1)	7.23 -7.10
H-Ar (2)	7.18 -7.04

Compound **6** / Protons	δ (multiplicity, J)
NH_Arg	8.48 (d, 7.9 Hz)
αH-Arg	4.27 (m)
βH-Arg	1.80 (m) ; 1.71 (m)
γH-Arg	1.59 (m)
δH-Arg	3.15 (m)
NH_guan	7.20 (m)
NH_Gly	8.50 (m)
αH-Gly	3.85 (m) ; 3.70 (dd, 15.8-6.2 Hz)
NH_Asp	8.95 (m)
αH-Asp	4.34 (m)
βH-Asp	2.74 (m) ; 2.59 (dd, 16.2-8.8 Hz)
DKP_NH4	8.22 (s)
DKP_NH10	8.01 (t, 5.8 Hz)
DKP_H9	3.88(m) ; 3.50 (m)
DKP_H3	4.35 (m)
DKP_H7	2.79 (dd, 13.8-4.5 Hz) ; 2.73 (m)
DKP_H6	4.25 (m)
CH_2-Bn	5.08 (m) ; 4.26 (m)
H-Ar	7.42-7.30

Compound **7** / Protons	δ (multiplicity, J)
NH_Arg	8.43 (d, 6.24 Hz)
αH-Arg	4.13 (m)
βH-Arg	1.72 (m) ; 1.60 (m)
γH-Arg	1.54 (m)
δH-Arg	3.12 (m)
NH_guan	7.16 (m)
NH_Gly	8.56 (m)
αH-Gly	3.75 (m) ; 3.64 (dd, 15.73-6.89 Hz)
NH_Asp	8.57 (m)
αH-Asp	4.48 (m)
βH-Asp	2.66 (dd, 16.54-7.33 Hz) ; 2.49 (dd, 16.54-7.80 Hz)
DKP_NH10	7.73 (dd, 8.93- 3.20 Hz)
DKP_H9	3.72 (m)- 3.26 (ddd, 14.55-8.60-3.20 Hz)
DKP_H3	4.04 (m)
DKP_H7	2.91 (dd, 15.02-6.38 Hz) ; 2.78 (dd, 15.02-1.91 Hz)
DKP_H6	4.43 (m)
CH_2-Bn (1)	5.16 (d, 17.32 Hz) ; 4.29 (d, 17.32 Hz)
CH_2-Bn (2)	5.21 (d, 15.97 Hz) ; 4.18 (d, 15.97 Hz)
H-Ar (1)	7.40-7.10
H-Ar (2)	7.40-7.10

STD and ^{1}H-NMR spectra of compounds 2-6

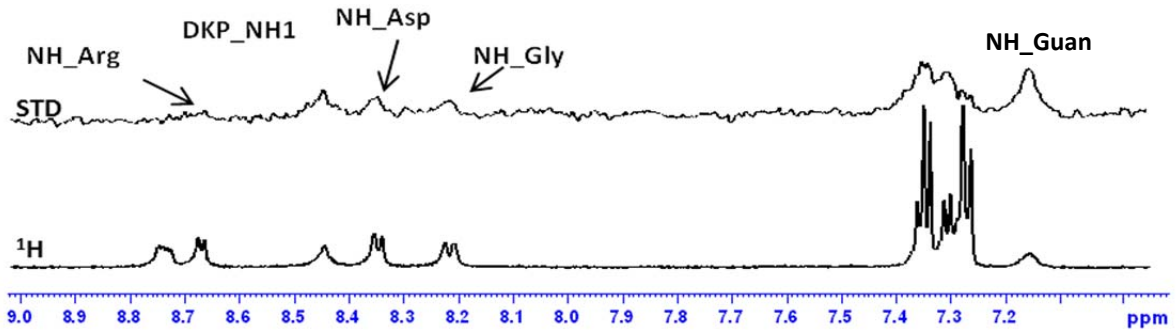

Figure S6. STD and ^{1}H-NMR low-field spectrum of compound **2** in buffer solution in presence of MDA-MB-231 cancer cells suspension at 283K.

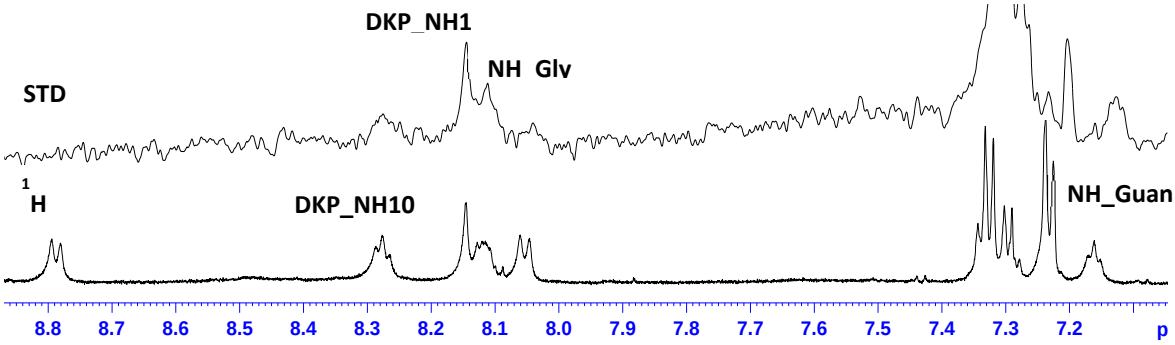

Figure S7. STD and ^{1}H-NMR low-field spectrum of compound **3** in buffer solution in presence of MDA-MB-231 cancer cells suspension at 283K.

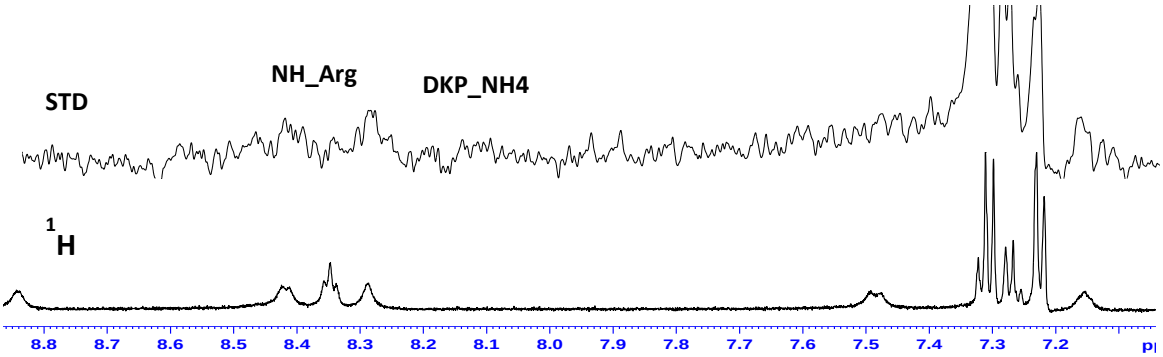

Figure S8. STD and ^{1}H-NMR low-field spectrum of compound **4** in buffer solution in presence of MDA-MB-231 cancer cells suspension at 283K.

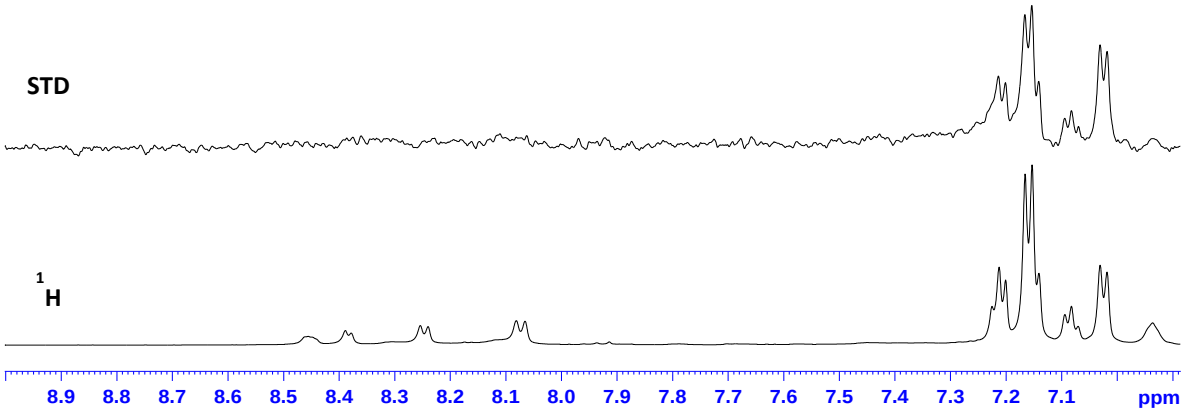

Figure S9. STD and ^{1}H-NMR low-field spectrum of compound **5** in buffer solution in presence of MDA-MB-231 cancer cells suspension at 283K.

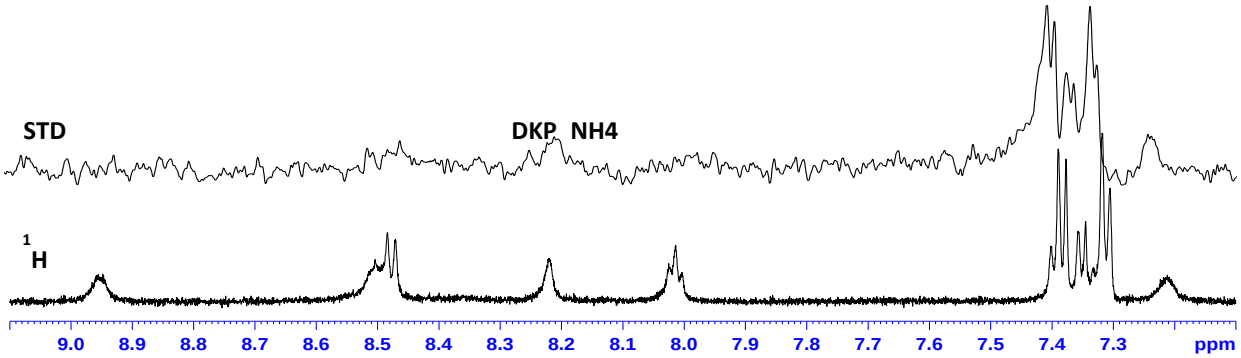

Figure S10. STD and ^{1}H-NMR low-field spectrum of compound **6** in buffer solution in presence of MDA-MB-231 cancer cells suspension at 283K.

Table of relative and absolute STD % values

Table S7. Relative percentages (%) and absolute (abs) STD values are reported for compounds **2-7**. The spectra were acquired in phosphate buffer solution (pH 7.2) in the presence of MDA-MB-231 cell suspension at T= 283 K.

Compound / Proton	**2**		**3**		**4**		**5**		**6**		**7**	
	%	abs	%	abs	%	abs	%	abs	%	abs	%	abs
NH_Arg	60	0,84			75	0,87					32	0,59
δH_Arg	14	0,20					15	0,17			11	0,20
NH-Guan	100	1,40	60	0,78	53	0,61	72	0,79	54	0,71	36	0,65
NH_Gly	36	0,50	69	0,91							23[a]	0,42[a]
αH_Gly	28	0,40					26	0,29	63	0,83	58	1,05
NH_Asp	36	0,50									23[a]	0,42[a]
H_Ar1	21	0,30	100	1,30	100	1,16	100	1,10	100	1,32	72	1,30
H_Ar2							100	1,10			72	1,30
DKP_NH1			77	1,01								
DKP_H3					54	0,64					78	1,40
DKP_NH4					67	0,77			51	0,68		
DKP_H7	28	0,40			97	1,12	100	1,10	34	0,43	54	0,98
DKP_H9	28	0,40			46	0,53	41	0,45	48	0,64	100	1,81
DKP_NH10			45	0,58							52	0,94

[a] Due to overlap of these signals, the observed values have been attributed to both protons.